

Phase resetting, phase locking, and bistability in the periodically driven saline oscillator: Experiment and model

Hortensia González,^{1,*} Humberto Arce,^{1,†} and Michael R. Guevara^{2,‡}

¹*Departamento de Física, Facultad de Ciencias, Universidad Nacional Autónoma de México, Apartado Postal 70-542, 04510 México, Distrito Federal, México*

²*Department of Physiology and Centre for Nonlinear Dynamics in Physiology and Medicine, McGill University, 3655 Sir William Osler Promenade, Montréal, Québec H3G 1Y6, Canada*

(Received 30 April 2008; published 18 September 2008)

The saline oscillator consists of an inner vessel containing salt water partially immersed in an outer vessel of fresh water, with a small orifice in the center of the bottom of the inner vessel. There is a cyclic alternation between salt water flowing downwards out of the inner vessel into the outer vessel through the orifice and fresh water flowing upwards into the inner vessel from the outer vessel through that same orifice. We develop a very stable (i.e., stationary) version of this saline oscillator. We first investigate the response of the oscillator to periodic forcing with a train of stimuli (period= T_p) of large amplitude. Each stimulus is the quick injection of a fixed volume of fresh water into the outer vessel followed immediately by withdrawal of that very same volume. For T_p sufficiently close to the intrinsic period of the oscillator (T_0), there is 1:1 synchronization or phase locking between the stimulus train and the oscillator. As T_p is decreased below T_0 , one finds the succession of phase-locking rhythms: 1:1, 2:2, 2:1, 2:2, and 1:1. As T_p is increased beyond T_0 , one encounters successively 1:1, 1:2, 2:4, 2:3, 2:4, and 1:2 phase-locking rhythms. We next investigate the phase-resetting response, in which injection of a single stimulus transiently changes the period of the oscillation. By systematically changing the phase of the cycle at which the stimulus is delivered (the old phase), we construct the new-phase—old-phase curve (the phase transition curve), from which we then develop a one-dimensional finite-difference equation (“map”) that predicts the response to periodic stimulation. These predicted phase-locking rhythms are close to the experimental findings. In addition, iteration of the map predicts the existence of bistability between two different 1:1 rhythms, which was then searched for and found experimentally. Bistability between 1:1 and 2:2 rhythms is also encountered. Finally, with one exception, numerical modeling with a phenomenologically derived Rayleigh oscillator reproduces all of the experimental behavior.

DOI: [10.1103/PhysRevE.78.036217](https://doi.org/10.1103/PhysRevE.78.036217)

PACS number(s): 82.40.Bj, 05.45.-a, 02.30.Oz

I. INTRODUCTION

When two or more oscillators are coupled together, 1:1 mutual synchronization as well as more complicated rhythms can arise. Analysis of this situation of bidirectional coupling, in which each individual oscillator both affects and is affected by the activity of the other oscillator, is difficult. A simpler situation that deserves to be understood is the case of unidirectional coupling, in which an external source periodically drives or stimulates a single oscillator [1]. In this situation, the oscillator will respond in a 1:1 fashion provided that two conditions are satisfied: (i) the period of the driving oscillator (T_p) must be sufficiently close to the intrinsic period of the driven oscillator (T_0), and (ii) the forcing amplitude must be sufficiently high when $T_p \neq T_0$. Should either of these two criteria not be met, 1:1 synchronization will be lost and replaced by some other periodic, quasiperiodic, or chaotic response [2].

When the forcing amplitude is sufficiently low, the response is well known: one has either a periodic (phase-locked) rhythm or an aperiodic (quasiperiodic) rhythm. In the two-parameter (stimulation-period–forcing-amplitude) plane, the former rhythms occur within areas called Arnol’d

tongues or resonance horns, while the latter occur on one-dimensional arcs that thread up between the Arnol’d tongues. This generic behavior has been seen in work on very many physical, chemical, and biological oscillators, in both experiment (e.g., [3–8]) and model (e.g., [2,9–19]).

Much richer behavior is seen at higher forcing amplitudes, where there can be period-doubling bifurcations, torus bifurcations, codimension-2 bifurcations, global bifurcations, bistability, cusps, and chaotic dynamics. Moreover, as T_p is changed systematically at some fixed forcing amplitude, there is not just one simple generic bifurcation sequence, as is the case at the lowest forcing amplitudes, where, e.g., the Arnol’d tongues are born and die in saddle-node bifurcations. Much of the behavior seen at higher forcing amplitudes remains to be systematically described experimentally and the corresponding theory worked out.

We thus decided to investigate systematically the response to periodic stimulation at higher forcing amplitude of a simple hydrodynamical oscillator: the saline oscillator. While the behavior of as many as 36 mutually coupled saline oscillators has been studied previously [20–24], there have been no studies of the unidirectional synchronization of a single saline oscillator. To help understand the organization of the synchronization rhythms, we conducted phase-resetting experiments in order to obtain a one-dimensional map, which is then iterated to predict the response to periodic stimulation [25]. We also carried out numerical simulations of the periodically forced two-variable Rayleigh oscillator, which has

*hgg@hp.fciencias.unam.mx

†jhar@hp.fciencias.unam.mx

‡michael.guevara@mcgill.ca

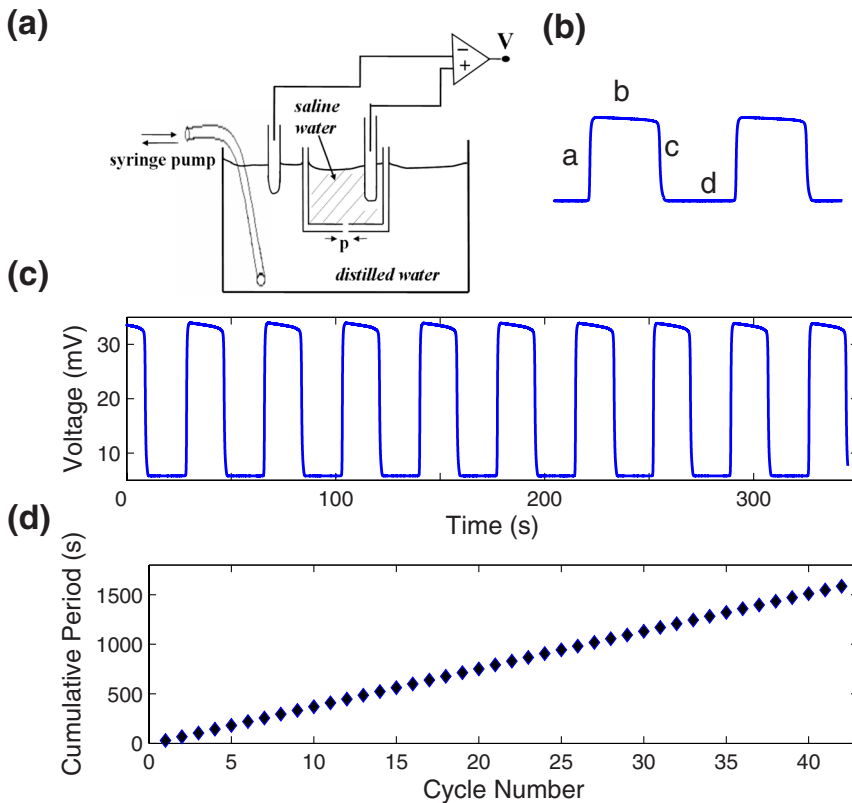


FIG. 1. (Color online) (a) Schematic diagram of the experimental setup. p denotes the pinhole at the bottom of the inner container. (b) Basal voltage oscillations which correlate with flux changes through pinhole. During phase b , distilled water flows upwards through the pinhole; during phase d , salt water flows downwards; during phases a and c there are flow reversals. (c) Voltage wave form recorded during several cycles of unperturbed activity. (d) Cumulative period for 42 consecutive cycles. Period (mean \pm s.d.) = 37.94 ± 0.59 s.

been shown to be a surprisingly realistic model of the saline oscillator [26]. Our interest in systems as simple as the saline oscillator is to gain insight into the phase-resetting and synchronization properties of much more complex biological oscillators (e.g., cardiac and neural pacemaker cells, circadian rhythms).

II. METHODS

A. Saline oscillator

The saline (or density) oscillator is a very simple system that was first described in 1970 by Martin, who discovered that a rhythmic oscillation of fluid flow was produced when a hypodermic syringe (without the plunger) was filled with saline solution, held in the vertical position, and then partially immersed in a beaker containing pure water [27]. Oscillations were also seen when the syringe was replaced with a tin can with a pinhole in its bottom. Many studies subsequently investigated the hydrodynamical mechanisms underlying the oscillation, using both experimental and modeling approaches (e.g., [21,26,28–36]).

Our experimental setup is illustrated in Fig. 1(a). The outer glass container, which was 9.7 cm high and 23 cm in inner diameter, contained 3.1 l of distilled, de-ionized water, so that the water had a depth of 7.5 cm. An acrylic plate with a hole in its center was placed across the top of the outer container to hold the inner cup in place. The inner plastic cup was 6 cm in inner diameter and 7.7 cm in height, and contained 90 ml of 3 M NaCl (175.5 g/l). The bottom of the cup was 4.1 cm above the bottom of the outer container. The pinhole in the center of the bottom of the inner cup [p in Fig.

1(a)] was 0.9 mm in diameter and 2.2 mm in length. A wooden plug was placed in the pinhole to prevent flow until the start of the experiment.

To initiate the oscillation, the wooden plug was removed. The salt water then began to flow downward through the pinhole because it was denser than the distilled water in the outer container (the Rayleigh instability [27]). A few minutes later the downward flow reversed so that distilled water from the outer container began to flow upward through the pinhole into the inner cup. After several tens of seconds this upward flow stopped, and then the salt water again began to flow downward. This cycle repeated thousands of times over many hours until the saline gradient was dissipated and the oscillation stopped. Part of the reason why the oscillation lasts so long is apparently that salt water sinks to the bottom of the distilled-water container, while distilled water rises to float on top of the salt water in the cup [21,34]. The density oscillator uses a fluid (water) containing an electrolyte (NaCl), and when there is a flow a voltage is generated which can be recorded using two Ag/AgCl₂ electrodes [Fig. 1(b)], one placed in the salt water and the other placed in the distilled water [Fig. 1(a)]. While the origin of the voltage variations is not completely clear, it appears to be due to streaming potentials [32,33], and it is known that changes in voltage are representative of changes in flow [23,31,32,36].

B. Volume pulse protocol

The oscillator was perturbed by infusing a fixed volume (3 ml) of distilled water into the bottom of the outer container and then withdrawing that same exact volume, using a syringe pump driving two 60-ml syringes in parallel (WPI

SP210iw infusion-withdrawal pump). This volume is only 0.1% of the total volume in the outer container. A fixed flow rate of 140 ml/min was used, so that the time to inject or withdraw a volume of 3.0 ml was 1.3 s, which is only a small fraction of the natural period of the oscillation (~ 35 s). The accuracy of this pump is rated by the manufacturer at $>99\%$ and the reproducibility at $\pm 0.1\%$. A computer-controlled interface was used to deliver these biphasic volume pulses either singly (to investigate phase resetting) or in a periodic fashion (to investigate phase locking). The rationale behind using a biphasic pulse is to prevent the stimulus itself from producing a long-lasting, cumulative effect on the volume—and thus the height—of the fluid. This is especially important for experiments in which long phase-locking runs, necessitating the delivery of many pulses, are made.

C. Data recording and analysis

A digital data-acquisition system was employed to record the voltage generated by the saline oscillator as well as a transistor-transistor logic (TTL) signal that indicated when the pump was infusing. A digital data recorder (InstruTech VR-10B [95]; 47.2 kHz sampling frequency, 14-bit resolution, DC-18 kHz frequency response) was used to record the signals in pulse-code modulated (PCM) format on a videocassette recorder and as a disk file on a PC (InstruTech VR-111 data interface board; decimation factor of 128 leading to an effective sampling interval of 2.71 ms). The data were further decimated by a factor of 3 and passed through a Gaussian digital low-pass filter with $\sigma=0.05$ [37]. To display, measure, and plot the data, we used ACQUIRE-5.0.1, REVIEW-5.0.1, and DATAACCESS-7.0.2 (Bruxon Corp. [96]), as well as custom-written MATLAB programs.

D. Numerical simulations

Numerical simulation runs of the Rayleigh oscillator were carried out using MATLAB and programs written in C and FORTRAN (~ 16 significant decimal digits). A forward Euler numerical integration scheme with a time step of 0.001 s was used.

III. EXPERIMENTAL RESULTS

A. The intrinsic oscillation

Figure 1(b) shows two cycles of the oscillation in voltage (V) recorded in the saline oscillator. The salt water starts to flow downwards through the pinhole at the time when phase b turns into phase c , with this downwards flow continuing during phase d . There is a flow reversal as phase d turns into phase a , and during phases a and b of the oscillation fresh water flows upwards through the pinhole, whereupon the cycle then repeats. Phase b lasts slightly longer than phase d , occupying $53\% \pm 0.9\%$ [mean \pm standard deviation (s.d.), 100 cycles] of the intrinsic period.

Under our experimental conditions, the intrinsic period at the start of the experiment is 35.3 ± 2.7 s (mean \pm s.d.; 46 runs made on 46 different days). Due to mixing of salt and fresh water, there is a gradual increase in the intrinsic period

that is generally less than 10% over a time period of ~ 10 h (see also [26]). Over a shorter period of time, the cycle-to-cycle fluctuations in the voltage V [Fig. 1(c)] and intrinsic period [Fig. 1(d)] are very slight, with the coefficient of variation (s.d./mean) of period being only 1.6% over the 42 cycles shown in Fig. 1(d).

B. Phase-locking rhythms

We investigated the response of the saline oscillator to perturbation with a periodic train of biphasic volume pulses delivered to the outer vessel, with the time between pulses being denoted by T_p . Each pulse consists of the infusion of 3 ml of distilled water into the outer container, followed immediately by withdrawal of that same volume. Since the oscillator recovers back to its intrinsic period very rapidly following the cessation of stimulation (see below), we allowed at least three unperturbed cycles to occur following the end of each periodic stimulation run as a recovery period, before restarting stimulation at a new value of T_p .

When T_p is shorter than T_0 , the intrinsic period of the oscillation, but not too much so, there is a 1:1 phase-locking rhythm in the steady state [Fig. 2(a): $T_p/T_0=0.6$], following a short start-up transient [the upper blue trace gives the voltage wave form, while the lower red trace indicates the first half of the biphasic volume pulse (volume injection)]. In a 1:1 rhythm there is one response associated with each stimulus, with the stimulus falling at the same point or phase in the cycle in different cycles. Following the cessation of stimulation, the period of the oscillator recovers back to its intrinsic period very quickly [e.g., for the run of Fig. 2(a), the period is 37.7 s on the cycle immediately following the cessation of stimulation, while T_0 is 37.1 s]. We denote this rhythm by 1:1s (slow) to distinguish it from a different 1:1 rhythm, 1:1f (fast), which we shall encounter below. As T_p is increasingly reduced, 1:1 rhythm is initially maintained, with a gradual decrease in the durations of both phases b and d . Phase d is shortened due to the fact that the stimulus pulse increases the hydrostatic pressure in the outer container to the point that a flow reversal occurs earlier than it otherwise would spontaneously.

Eventually, as T_p is reduced further, 1:1 phase locking can no longer be maintained and there is a transition to a 2:2 phase-locking rhythm, each cycle of which consists of two stimuli and two large-amplitude responses of different durations [Fig. 2(b): $T_p/T_0=0.5$]. We denote this rhythm by 2:2s to distinguish it from a different 2:2 rhythm (2:2f), which we shall encounter later. In an $N:M$ rhythm, there is a repeating cycle that consists of N stimuli and M responses, with each of the N different stimuli falling at its own characteristic point or phase in the cycle. Further reduction of T_p leads to a fall in the duration of the smaller of the two responses of the 2:2 rhythm until eventually a 2:1 phase-locking rhythm occurs, each cycle of which consists of two stimuli and only one large-amplitude response [Fig. 2(c): $T_p/T_0=0.3$]. In this case, every second stimulus [the even-numbered ones in Fig. 2(c)] shortens phase d by advancing the point in time at which the next flow-reversal (phase a) occurs. Reducing T_p further, a 2:2 rhythm, which we refer to

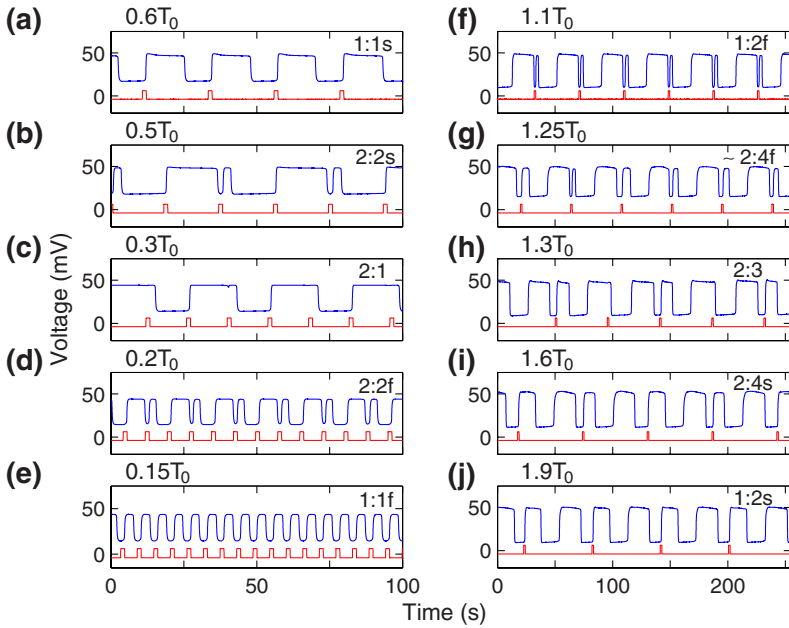


FIG. 2. (Color online) Top trace (blue) in each panel is the voltage recording; bottom trace (red) is the stimulus pulse train. Only the first half (volume injection) of each biphasic stimulus is shown. (a)–(e) Stimulation period (T_p) < intrinsic period (T_0). (a) 1:1s rhythm ($T_p/T_0 = 0.6$), (b) 2:2s rhythm ($T_p/T_0 = 0.5$), (c) 2:1 rhythm ($T_p/T_0 = 0.3$), (d) 2:2f rhythm ($T_p/T_0 = 0.2$), and (e) 1:1f rhythm ($T_p/T_0 = 0.15$). (f)–(j) $T_p > T_0$. (f) 1:2f rhythm ($T_p/T_0 = 1.1$), (g) $\sim 2:4f$ rhythm ($T_p/T_0 = 1.25$), (h) 2:3 rhythm ($T_p/T_0 = 1.3$), (i) 2:4s rhythm ($T_p/T_0 = 1.6$), and (j) 1:2s rhythm ($T_p/T_0 = 1.9$). Recordings in (a)–(e) and (f)–(j) obtained during experiments carried out on two different days. Note the time-scale change in (a)–(e) vs (f)–(j).

as 2:2f, occurs [Fig. 2(d): $T_p/T_0 = 0.2$]. Finally, as the shortest possible T_p is approached (there is an intrinsic lower limit on T_p set by the duration of the stimulus), a 1:1 rhythm, which we refer to as 1:1f, is seen [Fig. 2(e): $T_p/T_0 = 0.15$]. Thus, the sequence of rhythms seen as T_p is reduced from T_0 is $\{1:1s \rightarrow 2:2s \rightarrow 2:1 \rightarrow 2:2f \rightarrow 1:1f\}$.

We also investigated the response to periodic forcing with $T_p > T_0$. Figures 2(f)–2(j) show that as T_p/T_0 is increased, one sees the sequence $\{1:1s \rightarrow 1:2f \rightarrow 2:4f \rightarrow 2:3 \rightarrow 2:4s \rightarrow 1:2s\}$. So far, we have given the impression that only periodic rhythms are seen in our experiments. However, irregular rhythms are also seen, typically when T_p/T_0 is close to the border between two rhythms. Figure 2(g) shows an example: the rhythm here is close to a periodic 2:4f rhythm, which can be seen in other experimental runs. Due to the slight drift in the period of the oscillation that occurs over the course of a long experiment, the value of T_0 for each of the runs in Fig. 2 is taken from the last unperturbed cycle preceding that particular stimulation run.

C. Phase resetting

In situations in which the state point of the system returns to the limit cycle rapidly following the perturbation provided by a brief stimulus, it is possible to use the response to a single stimulus delivered at various phases of the cycle (the phase-resetting response) to predict the response to periodic perturbation [10,25,38]. The fact that both the period and amplitude of the oscillation are restored very quickly in the saline oscillator following a single stimulus (see below) is indicative of a rapid relaxation of the trajectory back to the limit cycle following a perturbation. We therefore investigated the phase-resetting response of the saline oscillator as a necessary first step in carrying out this predictive approach.

A single brief stimulus delivered to the saline oscillator transiently changes the period of the oscillation (“phase resetting”). We take the start of the cycle—which is arbitrary—to be midway through phase c [Fig. 1(b)], which

is termed the event marker. The coupling interval of the stimulus (T_c) is the time from this point to the end of the infusion phase, which is midway through the biphasic stimulus pulse [Fig. 3(a), top]. The cycle length of the perturbed cycle (T_1) is the time from the event marker immediately preceding the stimulus pulse to the event marker immediately following the stimulus. A stimulus falling late in the cycle, but not too late [Fig. 3(a), top], abbreviates the duration of phase b , resulting in a slight abbreviation of the perturbed cycle length. A stimulus falling during phase d , which occupies the first half of the cycle, causes an almost immediate flow reversal, producing a new large-amplitude event [Fig. 3(a), bottom left]. This event is brief in duration, and so T_1 is abbreviated. As the stimulus is delivered increasingly later on during phase d , the duration of the new event gradually increases, so that T_1 is increasingly less abbreviated. Finally, a stimulus that falls very late in the cycle prolongs the duration of phase b and so increases the length of the perturbed cycle [Fig. 3(a), bottom right].

There are thus three qualitatively different phase-resetting responses in Fig. 3(a). In Fig. 3(a), bottom left, the stimulus is injected during phase d , during which time salt water is flowing down through the pinhole. The first half of this stimulus—an injection of water into the outer container—causes the water level to rise in the outer container and thus raises the hydrostatic pressure at the lower side of the pinhole. The forcing amplitude used here is sufficiently high so that this rise causes a flow reversal, thus sharply abbreviating the cycle length. In Fig. 3(a), top, the stimulus is delivered during phase b of the cycle, during which time fresh water is flowing upwards through the pinhole. The effect of the stimulus is to increase the pressure at the lower side of the pinhole and so augment this upward flow. This in turn increases the height of the water column in the inner container and thus raises the hydrostatic pressure at the upper side of the pinhole. Hence, the time of the next flow reversal is advanced, and so the cycle length is abbreviated. Finally, in Fig. 3(a), bottom right, the stimulus is delivered very late in

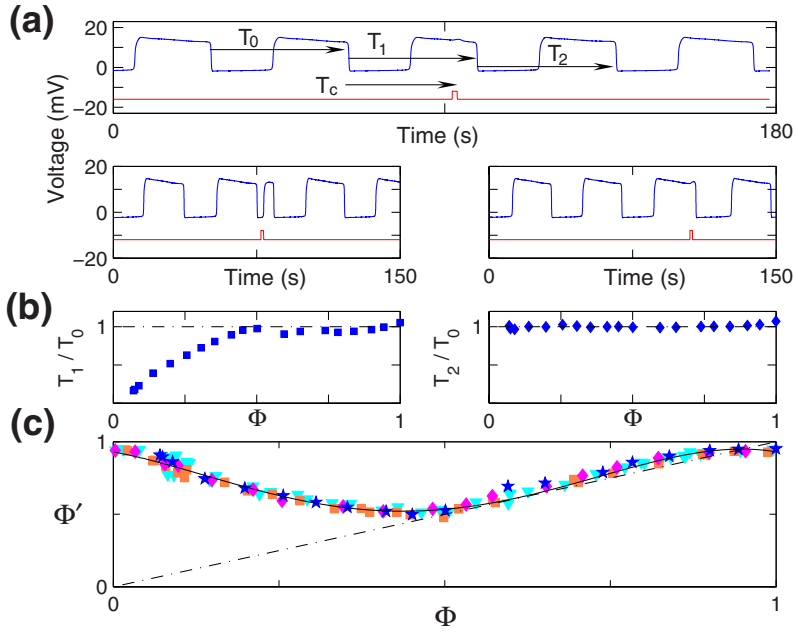


FIG. 3. (Color online) (a) Phase-resetting runs at three different values of the coupling interval T_c (top, 29.6 s; bottom left, 3.4 s; bottom right, 37.1 s). (b) Plots of T_1/T_0 vs old phase Φ ($=T_c/T_0$) (left) and T_2/T_0 vs Φ (right). (c) Plot of the new phase Φ' vs Φ . The curve is the phase transition curve (PTC), a quartic fit to the data points [$\Phi' = g(\Phi) = -6.20\Phi^4 + 10.77\Phi^3 - 3.72\Phi^2 - 0.85\Phi + 0.93$; $r^2 = 0.97$]. The four different sets of symbols are from experiments conducted on four different days; the blue star symbols are from the experiment shown in (a) and (b).

phase b , increasing the pressure in the outer container just before the reversal of the flow would normally occur, thus postponing the time of that reversal and lengthening the cycle length.

A stimulus falls at a particular phase of the cycle called the old phase (Φ), which is given by the normalized coupling interval T_c/T_0 , where T_0 is the length of the unperturbed cycle immediately preceding stimulus injection [Fig. 3(a), top]. Figure 3(b), left, is a plot of T_1/T_0 vs Φ and shows that while over most of the range of Φ ($0 < \Phi < 0.96$) there is a shortening of the cycle length, over a very short range of Φ ($0.96 < \Phi < 1$), there is instead a prolongation of the cycle length. The duration of the post-stimulation cycle is denoted by T_2 [Fig. 3(a), top], and plotting T_2/T_0 vs Φ [Fig. 3(b), right] demonstrates that the intrinsic period is reestablished very quickly following a perturbation.

The new phase (Φ'), defined as $\Phi' = 1 - T_1/T_0 + T_c/T_0$ (modulo 1) [39], is plotted in Fig. 3(c), which shows results from experiments made on four different days, separated by a period of ~ 3 years. These data demonstrate the reproducibility of the response, despite small day-to-day changes in wave form and period. A quartic polynomial fit is made to the lumped experimental data. However, this fit results in too large a difference between its values at $\Phi = 0$ and $\Phi = 1$. To help improve the match at the two ends of the curve, the fit was remade after adding 12 additional points to the original data set: the first six points of the data set were appended to the end of the original data set with Φ replaced by $\Phi + 1$, and the last 6 points of the data set were inserted before the start of the original data set, with Φ replaced by $\Phi - 1$. The resultant fit is shown by the curve in Fig. 3(c) and is called the phase transition curve (PTC): $\Phi' = g(\Phi)$.

The PTC reflects the three qualitatively different responses of the system. The decreasing left-hand branch ($0 \leq \Phi < 0.5$) corresponds to the type of response shown in Fig. 3(a), bottom left, where there is an abbreviation of T_1 to a value below T_0 ; the initial part of the rising right-hand branch ($0.5 < \Phi < 0.96$), with Φ' just barely greater than Φ ,

corresponds to Fig. 3(a), top, where there is only a small shortening of T_1 below T_0 ; and the part of the curve at the very right ($0.96 \leq \Phi < 1.0$), with Φ' just smaller than Φ , corresponds to Fig. 3(a), bottom right, where there is a slight prolongation of T_1 beyond T_0 .

D. One-dimensional map and predicted phase-locking rhythms

During periodic stimulation at arbitrary T_p , let the i th stimulus fall at a phase Φ_i . Assume that the effect of this stimulus is the same as had it been delivered as an isolated stimulus during a phase-resetting experiment. One then has

$$\Phi_{i+1} = g(\Phi_i) + T_p/T_0 \pmod{1}, \quad (1)$$

where $g(\Phi)$ is the PTC of Fig. 3(c) [25]. This equation is a one-dimensional finite-difference equation or map (“1D map”), allowing Φ_i to be iterated from any arbitrary initial condition, since T_p , T_0 , and g are known.

Figure 4(a) shows the bifurcation diagram obtained from Eq. (1). The solid blue curves are the stable period-1 and period-2 orbits, while the dotted red curves are the unstable period-1 orbits, all calculated directly from Eq. (1) [iterating Eq. (1) from 100 evenly spaced initial conditions at each value of T_p/T_0 with an increment in T_p/T_0 of 0.001 reveals that the only stable orbits that are present are period-1 and period-2 orbits]. As T_p/T_0 is decreased in Fig. 4(a), one obtains the sequence $\{1:1s \rightarrow 2:2s \rightarrow 2:1 \rightarrow 2:2f \rightarrow 1:1f\}$, which is exactly what is seen in the experiments [Figs. 2(a)–2(e)]. From the form of Eq. (1) (see Proposition 3 in [10]), as T_p/T_0 is increased, one then expects to see the sequence $\{1:1s \rightarrow 1:2f \rightarrow 2:4f \rightarrow 2:3 \rightarrow 2:4s \rightarrow 1:2s\}$, which again is exactly what is seen in the experiments [Figs. 2(f)–2(j)].

At $T_p/T_0 = 0.7$, there is a stable period-1 orbit on the map, corresponding to a 1:1s rhythm [Fig. 4(b), left]. With a decrease in T_p/T_0 , there is a supercritical period-doubling bifurcation that results in the 2:2s rhythm [Fig. 4(b), middle: $T_p/T_0 = 0.6$]. With a further decrease in T_p/T_0 , there is a

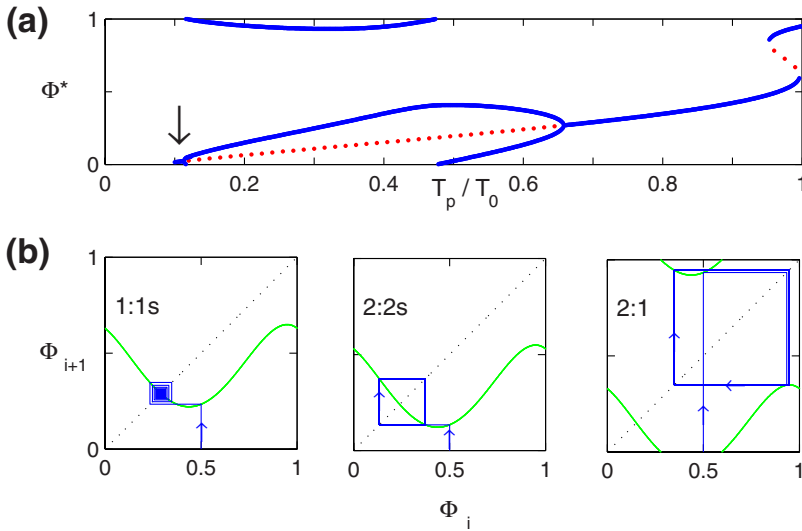


FIG. 4. (Color online) (a) Bifurcation diagram computed directly (i.e., not from iterations) from Eq. (1), using the quartic fit $g(\Phi)$ to the PTC [Fig. 3(c)]. Stable orbits, blue solid curves; unstable orbits, red dotted curves. Increment in $T_p/T_0=0.001$ (not all points computed are plotted). The sequence of rhythms as T_p/T_0 is increased is $\{1:1f \rightarrow 2:2f \rightarrow 2:1 \rightarrow 2:2s \rightarrow 1:1s\}$. Arrow indicates narrow range of T_p/T_0 over which there is a $1:1f$ rhythm. (b) Maps obtained from Eq. (1) corresponding to $1:1s$ rhythm (left, $T_p/T_0=0.7$), $2:2s$ rhythm (middle, $T_p/T_0=0.6$), and $2:1$ rhythm (right, $T_p/T_0=0.4$).

change in rotation number [10], resulting in a 2:1 rhythm [Fig. 4(b), right: $T_p/T_0=0.4$]. This change in rotation number occurs when one of the two points on the period-2 orbit crosses through zero: just before this zero crossing, this point has a phase just larger than zero [the lower point on the orbit in Fig. 4(b), middle], which corresponds to the production of a new large-amplitude response [see, e.g., Fig. 3(a), bottom left], while after the zero crossing, the phase is just less than one [the upper point of the orbit in Fig. 4(b), right], which corresponds simply to the prolongation of a preexisting large-amplitude event [see, e.g., Fig. 3(a), bottom right]. With still a further decrease in T_p/T_0 , there is another change in rotation number, leading to the conversion of the 2:1 rhythm into the 2:2f rhythm, and finally a reverse supercritical period-doubling bifurcation, leading to a $1:1f$ rhythm that exists only over a very narrow range of T_p/T_0 [arrow in Fig. 4(a)]. Note that there is a stable or unstable period-1 orbit present for all T_p [40].

E. 1:1a/1:1b bistability

At the extreme right of Fig. 4(a), there is a narrow range of T_p/T_0 , just below $T_p/T_0=1$, where three period-1 orbits

coexist. In the map [Fig. 5(a): $T_p/T_0=0.96$], there are two stable period-1 orbits (blue diamonds), corresponding to two stable 1:1 rhythms, as well as one unstable period-1 orbit (red circle), corresponding to an unstable 1:1 rhythm. Depending on the initial condition, one or the other of the two stable period-1 orbits [insets in Fig. 5(a)] is asymptotically approached. Bistability of two different 1:1 rhythms ($1:1a/1:1b$) is thus predicted. This suggests that if T_p/T_0 would be adjusted finely during the experiments to be within the putative bistable region, a well-timed perturbation should move the state point of the system from the limit cycle of the other 1:1 rhythm into the basin of attraction of the limit cycle of the other 1:1 rhythm. This theoretical prediction was verified experimentally in both directions [Fig. 5(b), left and right: $T_p/T_0=0.96$], with the arrows indicating the transient alteration of stimulus timing that provided the perturbation to induce the flip from one 1:1 rhythm to the other. To obtain either flip the stimulus timing must be well chosen; moreover, the timing was consistent with what is predicted from the map [Fig. 5(a)]. During the experimental $1:1a$ rhythm, the stimulus falls at a phase of ~ 0.5 , while during the $1:1b$ rhythm it falls at ~ 0.9 , which is again in excellent agreement

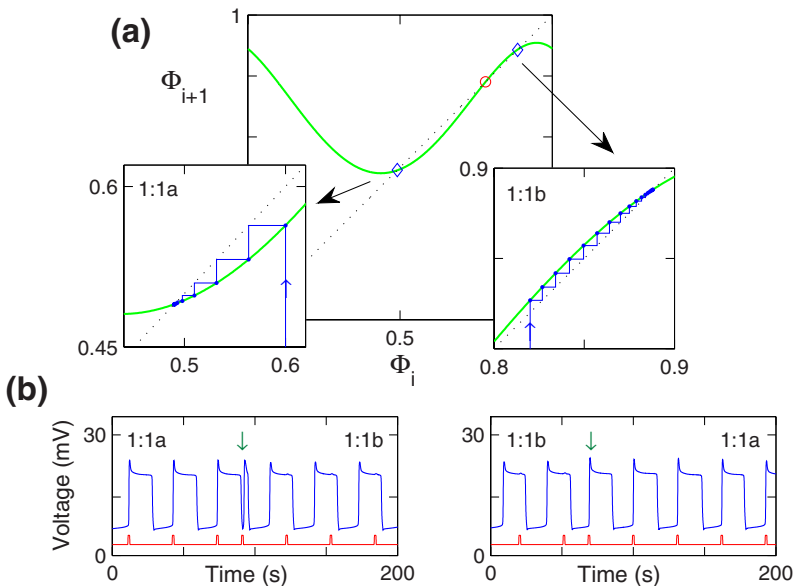


FIG. 5. (Color online) (a) Maps showing unstable period-1 orbit (red circle) and coexistence of two stable period-1 orbits (blue diamonds) at $T_p/T_0=0.96$. Depending on initial conditions, one or the other of the two stable period-1 orbits is asymptotically approached. (b) Experimental recording for $T_p/T_0=0.96$. Advancing the timing of one stimulus pulse (arrow) by a judiciously chosen amount flips the rhythm from $1:1a$ to $1:1b$ (left) or vice versa (right).

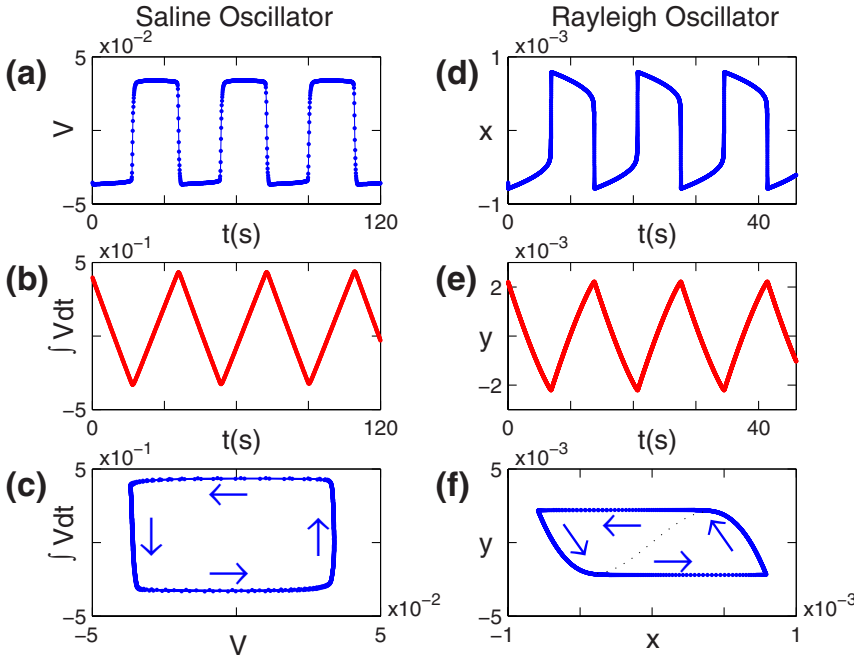


FIG. 6. (Color online) Left column: saline oscillator: (a) voltage, (b) voltage integral, and (c) reconstituted phase-plane trajectory. A slight offset has been added to the voltage trace to remove a slow drift in the integral trace. Right column: Rayleigh oscillator: (d) x -variable, (e) y -variable, and (f) phase-plane plot of the limit-cycle trajectory. The dotted curve shows the unstable leaf of the x -nullcline.

with the predictions of the map. We were unable to produce these flips experimentally when T_p/T_0 was reduced to 0.93, or when T_p/T_0 was increased to 0.99, again in agreement with the theoretical prediction that bistability exists only over a narrow range of T_p/T_0 [Fig. 4(a)].

IV. MODELING RESULTS

A. Rayleigh oscillator

Numerical integration of the Navier-Stokes equations reproduces many of the salient features of the intrinsic oscillation of the saline oscillator [26]. Working directly from the results of these simulations, one can reduce the problem to consideration of the Rayleigh oscillator

$$\frac{d^2y}{dt^2} = A \frac{dy}{dt} - B \left(\frac{dy}{dt} \right)^3 - \omega_0^2 y, \quad (2)$$

where y is the displacement of the height of the salt water in the inner container from its equilibrium height, $A=56$, $B=1.2 \times 10^8$, and $\omega_0^2=7$ [26] (see also [20,21,23,27,35,36] for other modeling of the saline oscillator involving low-dimensional ordinary differential equations).

As mentioned earlier, while it is still not known exactly which hydrodynamic variable corresponds to the voltage (V), the rapidly changing phases of V [phases a and c in Fig. 1(b)] line up closely in time with the flow reversals [31]. If we take V [Fig. 6(a)] as a measure of flow velocity through the orifice, then the integral of V [Fig. 6(b)] will be proportional to the fluctuations in the volume and thus in the height of the salt water. Indeed, Fig. 6(b) is similar to the experimental result and the result from the full Navier-Stokes simulation (Figs. 4 and 5 of [26], respectively), as is the phase-plane trajectory [compare Fig. 6(c) here with Fig. 6 in [26]].

We therefore decided to carry out phase-resetting and phase-locking simulations in the Rayleigh oscillator, apply-

ing the same biphasic stimulus as that employed in our experiments. One can rewrite Eq. (2) as

$$\frac{dx}{dt} = Ax - Bx^3 - \omega_0^2 y, \quad (3a)$$

$$\frac{dy}{dt} = x. \quad (3b)$$

The mean flow velocity at the orifice is thus now proportional to x . The time series of x and y , as well as the limit cycle of the unperturbed relaxation oscillator, are shown in Figs. 6(d)–6(f), respectively. The sets of traces in the two columns of Fig. 6 are similar, apart from the difference in time scale: the intrinsic period of our saline oscillator (~ 35 s) is ~ 2.5 times longer than that of the Rayleigh oscillator (13.8 s), mainly because the reduction from the Navier-Stokes simulations to the Rayleigh oscillator results in a sharp fall in the intrinsic period [26].

In the experiment, the biphasic stimulus pulse is an infusion and then a withdrawal of distilled water into the outer container at a fixed flow rate. This would be modeled by adding a biphasic pulse $F(t)$ to the right-hand side of the equation for the rate of change of the water height in the *outer* container. Using conservation of mass, one can show that this is equivalent to adding a term $G(t) = -[(r_o/r_i)^2 - 1]F(t)$ to the right-hand side of Eq. (3b), which governs the height of water in the *inner* container (r_i and r_o are the radii of the inner and outer containers, respectively). The negative sign in this term implies that the forcing of the inner container must be then carried out using a biphasic wave form with reversed polarities (i.e., withdrawal followed by infusion). We set the duration of the infusion and withdrawal phases in the model to be each 0.55 s, so that each of these phases lasts for 4% of the intrinsic period, as in the experiment.

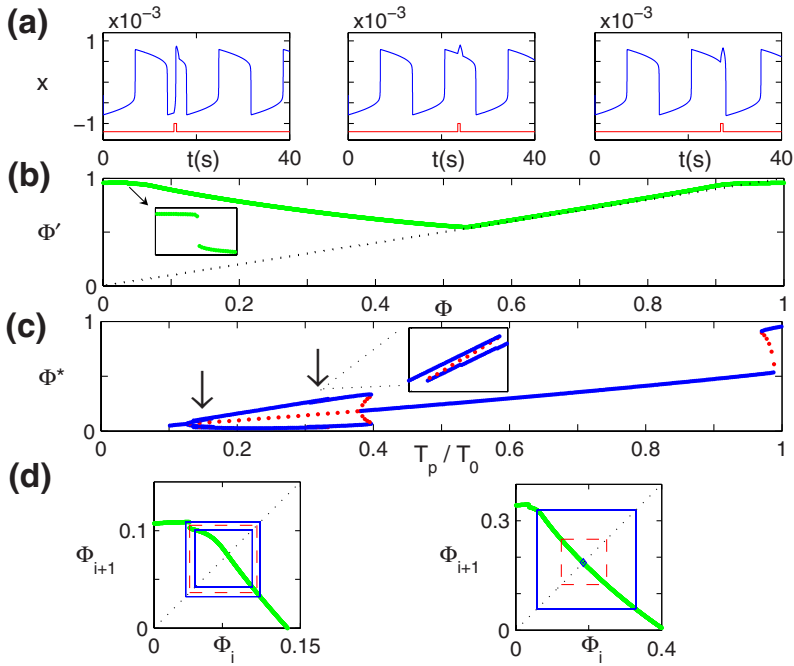


FIG. 7. (Color online) (a) Phase resetting runs at coupling interval $T_c=1.93$ s, 10.21 s, 13.66 s (left to right). (b) Phase transition curve. Number of data points=13 810. Original data points plotted, not a curve fitting the data points. Inset: close-up of a steep part of PTC where canardlike trajectories occur. (c) Bifurcation diagram computed directly (i.e., not from iterations) using a piecewise-linear fit to the data points in (b) for $g(\Phi)$ in Eq. (1). Solid blue curves, stable orbits; dotted red curves, unstable orbits. Increment in $T_p/T_0=0.001$ (not all points plotted). The sequence of rhythms as T_p/T_0 is increased is $\{1:1f \rightarrow 2:2 \rightarrow 1:1s\}$. Arrows indicate two regions of $2:2a/2:2b$ bistability (inset: close-up of the right bistable region). (d) Maps showing $2:2a/2:2b$ bistability (left, $T_p/T_0=0.15$) and $1:1/2:2$ bistability (right, $T_p/T_0=0.385$). Solid blue lines, stable period-2 orbits; dashed red lines, unstable period-2 orbits.

Note also that by making the change of variable, $z=y - \int G(t)dt$, it can be shown that

$$\frac{dx}{dt} = Ax - Bx^3 - \omega_0^2 z - \omega_0^2 \int G(t)dt, \quad (4a)$$

$$\frac{dz}{dt} = x, \quad (4b)$$

so that forcing the oscillator by adding a biphasic square pulse to the right-hand side of Eq. (3b) is equivalent to adding a monophasic positive triangular pulse to the right-hand side of Eq. (3a).

B. Phase resetting of the Rayleigh oscillator

Figure 7(a) shows three phase-resetting runs. When the stimulus is delivered relatively early in the cycle, during phase d , there is an almost immediate flow reversal [Fig. 7(a), left], as in the saline oscillator [Fig. 3(a), bottom left]. The same pulse delivered later in the cycle, during the earlier part of phase b , produces a shortening of that phase of the cycle [Fig. 7(a), middle], as in the experiment [Fig. 3(a), top], while if delivered sufficiently late in phase b , it produces a prolongation of that phase [Fig. 7(a), right], as in the experiment [Fig. 3(a), bottom right]. The amplitude of both components of the biphasic pulse added to the right-hand side of Eq. (3b) to represent the stimulus was empirically chosen to be 0.01 in order to yield a PTC [Fig. 7(b)] comparable to that of the experiments [Fig. 3(c)].

In Fig. 7(b), for $0 < \Phi < 0.05$, the PTC has a very small negative slope, except in a neighborhood of $\Phi=0.036$, where there is a very small abrupt jump with very large negative slope that is not appreciable on the scale of this figure (see inset). This jump is only an apparent discontinuity, since finer computation reveals that canardlike trajectories are seen

within this region, producing a very negative slope in the PTC. At $\Phi=0.54$ there is a rather abrupt change in the slope of the PTC from negative to positive; for $0.54 < \Phi < 0.91$, Φ' just barely exceeds Φ and the slope of the PTC is slighter >1 ; for $0.91 < \Phi < 1$, the PTC has a positive slope <1 ; and for $\Phi > 0.95$, $\Phi' < \Phi$. The PTC of the Rayleigh oscillator thus resembles closely the experimental PTC of Fig. 3(c) in terms of its overall shape. Given the degree of noise in the experimental system, as reflected in the scatter of data points in Fig. 3(c), it would be exceedingly difficult—indeed, probably impossible—to provide experimental evidence for the canardlike behavior seen in the noise-free model on the miniscule scale of the inset of Fig. 7(b).

C. One-dimensional map from the Rayleigh oscillator

As for the experiments, we carried out iterations of Eq. (1) using the PTC of the Rayleigh oscillator [Fig. 7(b)]. The phase-resetting data in Fig. 7(b) is composed of 13 810 data points, and linear interpolation between these points was used to generate a piecewise-linear function g in Eq. (1). Using an increment in T_p/T_0 of 0.001, at each value of T_p/T_0 , 1000 iterations were made from each of 100 evenly spaced initial conditions in the interval $[0,1)$. Only period-1 and period-2 stable orbits were found. Figure 7(c) shows the bifurcation diagram computed, not from iteration of Eq. (1), but rather by direct numerical calculation of period-1 and period-2 orbits from that equation (solid blue curves, stable; dotted red curves, unstable).

At the right of Fig. 7(c), an unstable period-1 branch links the two bistable period-1 branches corresponding to $1:1a$ and $1:1b$ rhythms; this bistability had been found earlier in the experiments [Fig. 5(b)] and in the experimental map [Figs. 4(a) and 5(a)]. Towards the left in Fig. 7(c), another unstable period-1 branch links the stable period-1 branches corresponding to $1:1s$ and $1:1f$ rhythms, as in the experi-

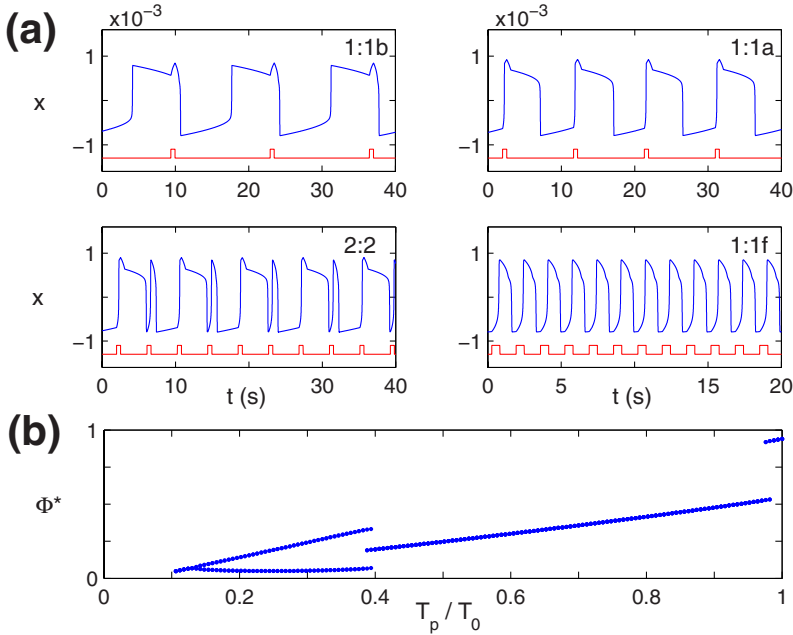


FIG. 8. (Color online) (a) Phase-locking rhythms. Top left, 1:1*b* rhythm ($T_p/T_0=0.98$); top right, 1:1*a* rhythm ($T_p/T_0=0.7$); bottom left, 2:2 rhythm ($T_p/T_0=0.3$); bottom right, 1:1*f* rhythm ($T_p/T_0=0.12$; note the change in time scale). (b) Bifurcation diagram. The phase of the oscillation at delivery of the stimulus pulse is plotted on the ordinate. Increment in $T_p/T_0=0.001$ (not all points computed are plotted). The total simulation time was 1.47×10^3 s, except in the region of the 1:1*a*/1:1*b* bistability where it was 1.47×10^4 s and in the region of the 1:1/2:2 bistability where it was 1.47×10^5 s. Initial conditions at each T_p/T_0 are 100 equally spaced points on the limit cycle, and only the last 20 points are plotted for each of these 100 runs made at each value of T_p/T_0 .

mental map [Fig. 4(a)]. The transition from the 1:1*f* rhythm to the 2:2 rhythm at $T_p/T_0=0.125$ is due to a supercritical period-doubling bifurcation, as in the experimental map [Fig. 4(a)]. However, the transition from a 1:1*s* rhythm to a 2:2 rhythm is associated with a subcritical period-doubling bifurcation that occurs at $T_p/T_0=0.38$. This finding is in contrast to the experimental map [Fig. 4(a)], where the bifurcation is supercritical (more about this difference later). Another discrepancy with respect to the experiments (Fig. 2) and the experimental map [Fig. 4(a)] is that a 2:1 rhythm is not seen.

The two arrows in Fig. 7(c) indicate two regions where there is bistability between two different period-2 orbits (corresponding to two different 2:2 rhythms), with the inset showing a close-up of the part of the upper branch of the bifurcation diagram indicated by the right-hand arrow: there is an unstable period-2 branch linking two stable period-2 branches (a similar configuration holds for the left-hand bistable region). Figure 7(d), left, shows an example of the map found in the bistable region indicated by the left arrow in Fig. 7(c) ($T_p/T_0=0.15$): there are two stable period-2 orbits (solid blue lines) and one unstable period-2 orbit (dashed red lines), with the latter acting as a separatrix to divide the basins of attraction of the two stable orbits. The leftmost point of the unstable period-2 orbit lies on the part of the map where the slope is very negative due to the existence of canardlike solutions on the PTC [inset of Fig. 7(b)]. This orbit could not be unstable—and the 2:2*a*/2:2*b* bistability would not exist—in the absence of this steep, negatively sloped range of the PTC (from the chain rule, the product of the slopes of the map at the two unstable period-2 points has to be >1 in absolute value for that orbit to be unstable). This steep region is similarly involved in generating the region of bistability indicated by the right-hand arrow in Fig. 7(c). Although this jump appears to be miniscule, its existence is crucial in allowing 2:2*a*/2:2*b* bistability to exist over two quite large ranges of T_p/T_0 in Fig. 7(c).

D. Phase-locking rhythms in the Rayleigh oscillator

We next carried out direct numerical integration to investigate the phase-locking rhythms in the Rayleigh oscillator for $0.1 \leq T_p/T_0 \leq 1.0$, with an increment in T_p/T_0 of 0.001. Figure 8(a) shows the rhythms found as T_p is decreased: 1:1*b* (upper left), 1:1*a* (upper right), 2:2 (lower left), and 1:1*f* (lower right). To search for bistability, at each value of T_p/T_0 , we carried out 100 runs, with the first stimulus of each run being injected at one of 100 evenly spaced points on the limit cycle. In the bifurcation diagram of Fig. 8(b), we plot the phases ϕ^* in the cycle at which the stimuli are injected from all 100 runs made at each value of T_p/T_0 (the last 20 points of each run are plotted).

Thus, as T_p/T_0 is decreased, one has the sequence of rhythms $\{1:1s \rightarrow 2:2 \rightarrow 1:1f\}$. In agreement with the prediction of the map [Fig. 7(c)], but in contrast to experiment (Figs. 2 and 4), a 2:1 rhythm is not seen. However, it is likely that with tiny changes in parameters, the lower point on the period-2 orbit in Fig. 8(b) would dip below $\phi=0$, thus yielding a 2:1 rhythm. Figure 8(b) shows that over a small range of T_p/T_0 there is 1:1*a*/1:1*b* bistability, as in the experiments [Fig. 5(b)], the experimental map [Figs. 4(a) and 5(a)], and the map from the Rayleigh oscillator [Fig. 7(c)]. But the 2:2*a*/2:2*b* bistability predicted from the map [Fig. 7(c)] is not found. Given the otherwise excellent agreement between Figs. 7(c) and 8(b), it is again likely that with tiny changes in parameters, 2:2*a*/2:2*b* bistability would be seen. For $T_p/T_0 > 1$, we see the sequence $\{1:1 \rightarrow 1:2f \rightarrow 2:4 \rightarrow 1:2s\}$, which again agrees with the 1D map predictions.

E. 1:1*s*/2:2*s* bistability

The results of both the numerical integration runs [Fig. 8(b)] and the iterations of the map [Fig. 7(c)] in the Rayleigh oscillator indicate that there is a range of 1:1*s*/2:2*s* bistability, which is a consequence of the period-doubling bifur-

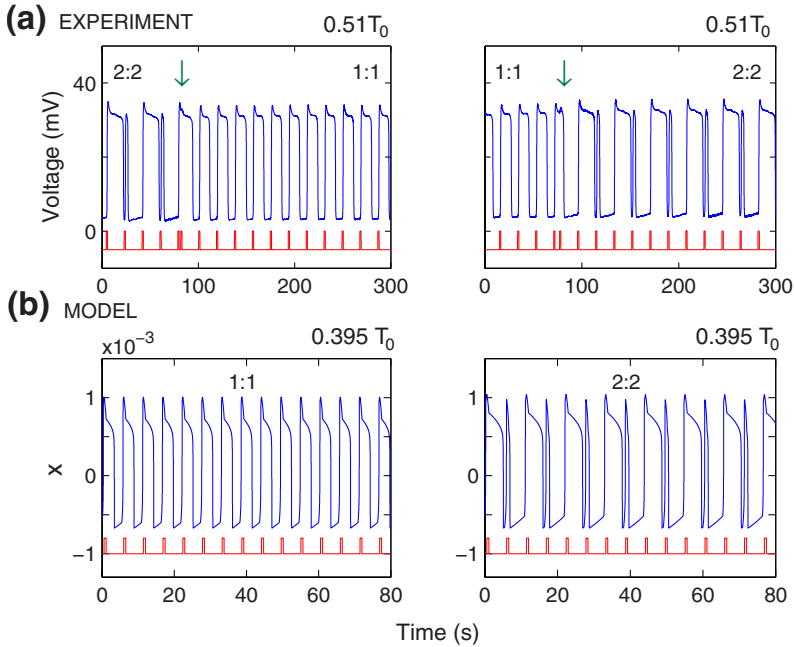


FIG. 9. (Color online) (a) Saline oscillator: advancing the timing of one stimulus pulse (arrow) by a correct amount flips the rhythm from 2:2 to 1:1 rhythm (left) or vice versa (right). $T_p/T_0=0.51$. (b) Rayleigh oscillator: coexisting 1:1s (left) and 2:2s (right) rhythms at $T_p/T_0=0.395$. Initial conditions: first stimulus injected at $\Phi=0.1$ (left) and $\Phi=0.5$ (right).

cation from 1:1s rhythm being subcritical [Fig. 7(d), right shows the coexisting stable period-1 and period-2 orbits, separated by an unstable period-2 orbit]. This bistability was not predicted from the experimental map [Fig. 4(a)], where the period-doubling bifurcation was supercritical. We nevertheless decided to search for this bistability in the experiments. In the saline oscillator, one can indeed flip the 2:2s rhythm to the 1:1s rhythm [Fig. 9(a), left] or vice versa [Fig. 9(a), right] by a carefully chosen transient advance in the timing of stimulation (arrows), as in the case of the 1:1a/1:1b bistability earlier described [Fig. 5(b)]. The two corresponding bistable rhythms in the Rayleigh oscillator [Fig. 9(b)] look remarkably similar to those in the saline oscillator [Fig. 9(a)].

F. Effect of different fits to the PTC on the bifurcation diagram

The 1D map correctly predicts the sequence of rhythms seen in the saline oscillator [Figs. 2(a)–2(e) vs Fig. 4(a)] as well as the 1:1a/1:1b bistability [Fig. 5(b) vs Figs. 4(a) and 5(a)]. The one major discrepancy is the prediction that the 2:2s rhythm should arise out of the 1:1s rhythm via a supercritical period-doubling bifurcation (Fig. 4), which is not in agreement with the experimental result demonstrating the existence of a subcritical bifurcation [Fig. 9(a)]. The period-doubling bifurcation is also subcritical in the Rayleigh oscillator, in both the phase-locking runs [Figs. 8(b) and 9(b)] and the map [Fig. 7(c)].

Since the two maps that predict super- and subcritical bifurcations (in the saline and Rayleigh oscillators, respectively) come from PTCs that are very similar [compare Fig. 3(c) with Fig. 7(b)], it is clear that some very subtle, seemingly insignificant, change in the PTC can convert the period-doubling bifurcation from super- to subcritical or vice versa. For example, fitting the PTC from the Rayleigh oscillator with a quartic polynomial (as in the experiments [Fig.

3(c)]) results in the subcritical period-doubling bifurcation at $T_p/T_0 \sim 0.4$ in Fig. 7(c) becoming supercritical, with the period-doubled branch of the bifurcation diagram resembling very much that obtained in the experimental work [Fig. 4(a)]. We thus tried other functional forms for the fit to the saline oscillator PTC (e.g., sine-wave, piecewise-linear-exponential forms), but in all cases the bifurcation remained supercritical. However, in the case of the piecewise-linear-exponential fit [Fig. 10(a) shows this fit (thin red curve) together with the raw data (solid circles); the original quartic fit of Fig. 3(c) is also shown for comparison (thick blue curve)], while the bifurcation remains supercritical, the period-doubled branch emerges in a much steeper fashion [contrast Fig. 10(b) with Fig. 4(a)]. It is thus quite likely that further small changes in the exact functional form of the fit would lead to the bifurcation becoming subcritical, which would then produce agreement with the experimental result [Fig. 9(a)]. However, it is difficult to offer a solid justification for making such subtle changes in the functional form of the fit, since all such changes would result in curves lying within the scatter of the data points [Fig. 10(a)].

When the period-doubling bifurcation is subcritical there are two coexisting stable periodic orbits: one of period-1 and the other of period-2 [e.g., Fig. 7(d) right]. Since bistability cannot exist when the Schwarzian derivative of a map is negative [41], which is the case for our quartic polynomial, piecewise-linear-exponential, and sine-wave fits, this explains why a subcritical period-doubling bifurcation cannot be obtained using these particular fits.

V. DISCUSSION AND CONCLUSIONS

A. Phase-locked rhythms with high-amplitude forcing

Much of the experimental and modeling work with high-amplitude forcing has been carried out hitherto on biological rather than physical systems. As T_p is decreased below T_0 ,

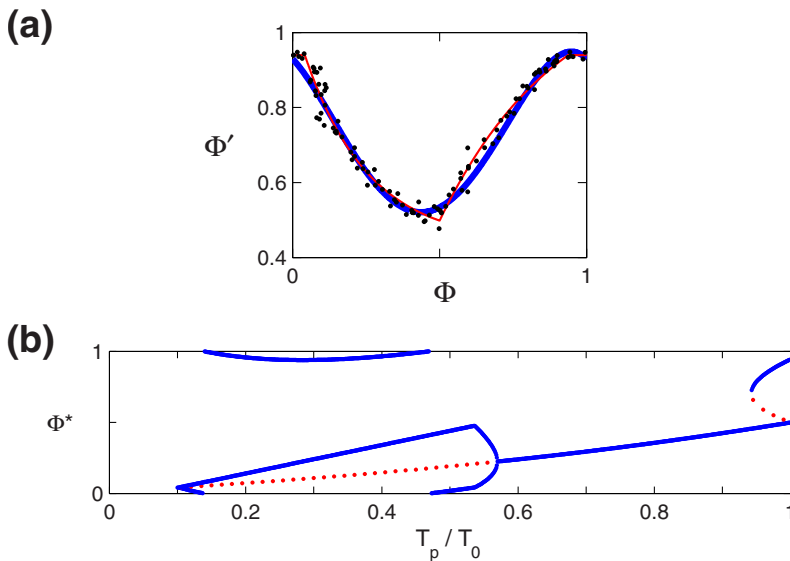


FIG. 10. (Color online) (a) Phase-resetting data from saline oscillator (symbols) with quartic fit (thick blue curve) and piecewise-linear-exponential fit (thin red curve). For the piecewise-linear-exponential fit, $g(\phi)=0.94$, $0 \leq \phi \leq 0.04178$; $g(\phi)=0.43842 + 9.31286e^{-(\phi+0.58866)/(0.2158)}$, $0.04178 < \phi \leq 0.50017$; $g(\phi)=1.17473(1 - e^{-2.41891(\phi-0.27194)})$, $0.50017 < \phi \leq 0.9377$; and $g(\phi)=0.94$, $0.9377 < \phi < 1.0$. (b) Bifurcation diagram constructed using Eq. (1) and the piecewise-linear-exponential $g(\phi)$ from (a). Increment in $T_p/T_0 = 0.001$ (not all points computed are plotted). Solid blue curves, stable orbits; dotted red curves, unstable orbits.

we encounter the sequence of rhythms $\{1:1s \rightarrow 2:2s \rightarrow 2:1 \rightarrow 2:2f \rightarrow 1:1f\}$ (Fig. 2). The $\{1:1 \rightarrow 2:2 \rightarrow 2:1\}$ sequence is seen with high-amplitude forcing in a very simple limit-cycle oscillator [10] and in the prototypical two-variable FitzHugh-Nagumo model of an excitable, but not spontaneously oscillating, system [42–44]. The 2:2 rhythm has been much studied in cardiac tissue, where it is called “alternans.” The $\{1:1 \rightarrow 2:2\}$ transition occurs in cardiac oscillators [8,45,46] as well as in excitable cardiac tissue (in both experiments [47–55] and in ionic models [49,52,56–61]). A further decrease in T_p typically converts the 2:2 rhythm into a 2:1 rhythm in both spontaneously active (e.g., [8,45,46]) and excitable (e.g., [48,49,51,54]) systems, as well as in ionic models [49,52,56,57,59,60]. However, several other possibilities exist in excitable systems: there can be (i) a reversion back to a 1:1 rhythm (experiment [55], ionic model [58,61]), (ii) a second period-doubling bifurcation leading to a 4:4 rhythm [50,53], (iii) a torus bifurcation leading to amplitude-modulated 2:2 rhythms [53], or (iv) a direct transition to chaos [42]. Indeed, the first possibility is what is seen in the Rayleigh oscillator at the stimulus amplitude used here (Fig. 8).

With $T_p > T_0$, we obtain the sequence $\{1:1s \rightarrow 1:2f \rightarrow 2:4f \rightarrow 2:3 \rightarrow 2:4s \rightarrow 1:2s\}$ (Fig. 2). Transitions in which only period-1 and period-2 rhythms occur between 1:1 and 1:2 rhythms have been seen in forced oscillators: e.g., the sequence $\{1:1 \rightarrow 2:2 \rightarrow 2:3 \rightarrow 2:4 \rightarrow 1:2\}$ [8,10].

B. Bistability involving period-1 and period-2 rhythms

Bistability (and the resultant hysteresis) in periodically forced systems has a long history in both the physical and biological worlds (e.g., [1,62]). In both the saline and Rayleigh oscillators, we see both $1:1a/1:1b$ bistability [Figs. 4(a), 5, 7(c), and 8(b)] and $1:1/2:2$ bistability [Figs. 7(c), 8(b), and 9]. $1:1a/1:1b$ bistability occurs experimentally in forced electrical and electrochemical systems [63,64], and two stable period-1 rhythms can coexist in simple models of periodically forced oscillatory and excitable systems [19,42,44,64,65]. $1:1/2:2$ bistability occurs in a convex uni-

modal 1D map with a positive Schwarzian derivative [66], as well as in far more complex ionic models of excitable cardiac tissue [52,57,59,67]. While a third form of bistability, $2:2a/2:2b$ bistability, was predicted to exist in the Rayleigh oscillator from the 1D map [arrows in Fig. 7(c)], this was not seen in the corresponding numerical integration runs [Fig. 8(b)]. Particularly interesting in this context is the fact that the unstable period-doubled limit cycle in the forced differential equation, corresponding to the unstable period-2 solution that is the separatrix in the map [Fig. 7(d), left], is then predicted to be a canard. There is evidence in experimental and modeling work for $2:2a/2:2b$ bistability [47,56,57,68], as well as for two other forms of bistability and hysteresis involving 1:1, 2:2, and 2:1 rhythms: $1:1/2:1$ bistability [8,42–44,48,49,54,59,60,62,65,68–73] and $2:2/2:1$ bistability [42–44,48,49,54,56,57,60,68].

C. Influence of the forcing amplitude on classes of phase-locking rhythms

At the lowest forcing amplitudes, the 1D map is a degree-1 invertible circle map, resulting in the periodic-quasiperiodic sequence corresponding to interleaved Arnol’d tongues and quasiperiodic dynamics (e.g., [2–5,8,11,12,15,17]). As forcing amplitude is raised, there is a transition to a degree-1 noninvertible circle map (e.g., [3]), and many Arnol’d tongues, after first widening, tend to split, narrow, and eventually disappear, with there being frequently an overlapping of tongues that produces bistability; in addition, torus bifurcations, period-doubling bifurcations, global bifurcations, and chaos can occur [2,6,7,9–19,65,68,69,71,74–80]. At a sufficiently high forcing amplitude, the PTC and the 1D map of Eq. (1) are of topological degree zero [6,10,39,81–85], and iteration of such a map can produce bistability, period-doubling bifurcations, and chaos [2,6,10,46,82,86]. As the amplitude is raised still further, the PTC and thus the map tend to flatten, so that higher-order rhythms are lost, leaving behind only period-1 and period-2 rhythms (sometimes only a period-1 rhythm) [6,10,13,15,40,46,75]. In the saline and Rayleigh oscillators

[Figs. 3(c) and 7(b)], the amplitude is sufficiently high so that the PTC and the map are of degree zero, and we encounter only period-1 and period-2 rhythms [Figs. 2, 4(a), 7(c), and 8(b)]. In preliminary work at lower forcing amplitudes in both oscillators, we see higher-order rhythms in the maps, as well as in the parallel phase-locking runs (e.g., 3:2, 3:1 rhythms).

D. Excitable vs spontaneously active systems

Several of the reports mentioned in the discussion above are on quiescent, excitable systems in which the unforced system does not possess a limit cycle. Indeed, much of the more complicated phenomenology mentioned above can be seen in such systems [6,43,44,51,70,87–89], as well as in periodically forced anharmonic oscillators (e.g., [90,91]). With high-amplitude forcing at small T_p , the fact that the system might be oscillating is not significant, since excitation will be produced by a stimulus before there can be a spontaneous excitation. In excitable systems, the analysis of the $\{1:1 \rightarrow 2:2 \rightarrow 2:1\}$ sequence typically involves a discontinuous two-branched interval map rather than a degree-zero circle map (e.g., [48,56,57,60]). The sequence $\{1:1 \rightarrow 2:2 \rightarrow 2:1\}$ and $1:1/2:2$ bistability can also be seen in excitable systems when a parameter other than T_p is changed: e.g., decreasing the excitability, which can be viewed as being equivalent to decreasing the forcing amplitude [67,92].

E. Ordinary vs partial differential equations

The recordings from the saline oscillator bear an uncanny resemblance to recordings of action potentials from cells in the heart and could be mistaken for such should absolute time and voltage scales be suppressed. In both cases, the system is properly described by a partial differential equation. It is most interesting that in both cases the dynamics can be reduced to the study of ordinary differential equations. This fact undoubtedly reflects the existence of an iner-

tial manifold in the system [93]. Perhaps even more surprising is the ability to successfully reduce analysis of the dynamics further to consideration of a 1D map. Indeed, it is possible on occasion to obtain a 1D map directly from simulations of a forced partial differential equation (e.g., [56,67]).

F. Super- vs subcritical period-doubling bifurcation

The 2:2 rhythm seen with high-amplitude forcing arises out of the 1:1 rhythm via a period-doubling bifurcation. While in some instances this bifurcation is reported to be supercritical (e.g., [10,40,46,48,54,56,75,94]), at other times it is reported to be subcritical (e.g., [59]). However, within a given system, both super- and subcritical bifurcations can be found, depending on parameter values (e.g., stimulus amplitude) [16,43,44,57,60,65]. Indeed, this existence of both types of bifurcation in a single system appears to be a generic feature of forced oscillators [16]. As driving frequency is further increased, the 2:2 rhythm can then be replaced by any one of several rhythms: e.g., 1:1, 2:1, 4:4, or amplitude-modulated 2:2 rhythm (references in Sec. V A above). It remains to be seen whether these different transitions all have a natural place in a single universal global bifurcation diagram (e.g., they might be seen at different forcing amplitudes) or whether they are due to intrinsic differences between different systems.

ACKNOWLEDGMENTS

This work was supported by grants to H.A. and H.G. from PAPIIT-UNAM (IN109307-2) and to M.R.G. from the Canadian Institutes of Health Research (Grant No. MOP-43846). We thank Jaime García Ruiz for expert technical help in running the experiments and with data analysis, Ricardo Pérez Martínez and Gabriela Arriola Cadena for help in preliminary experiments, and Huguette Croisier for helpful conversations.

-
- [1] B. van der Pol and J. van der Mark, *Nature (London)* **120**, 363 (1927).
 [2] L. Glass, *Nature (London)* **410**, 277 (2001).
 [3] L. Glass, M. R. Guevara, J. Belair, and A. Shrier, *Phys. Rev. A* **29**, 1348 (1984).
 [4] M. Eiswirth and G. Ertl, *Phys. Rev. Lett.* **60**, 1526 (1988).
 [5] M. R. Guevara, A. Shrier, and L. Glass, *Am. J. Physiol.* **254**, H1 (1988).
 [6] M. Dolnik, J. Finkeová, I. Schreiber, and M. Marek, *J. Phys. Chem.* **93**, 2764 (1989).
 [7] D.-R. He, D.-K. Wang, K.-J. Shi, C.-H. Yang, L.-Y. Chao, and J.-Y. Zhang, *Phys. Lett. A* **136**, 363 (1989).
 [8] M. R. Guevara, A. Shrier, and L. Glass, in *Cardiac Electrophysiology: From Cell to Bedside*, 1st ed., edited by D. P. Zipes and J. Jalife (Saunders, Philadelphia, 1990), p. 192.
 [9] K. Tomita and T. Kai, *J. Stat. Phys.* **21**, 65 (1979).
 [10] M. R. Guevara and L. Glass, *J. Math. Biol.* **14**, 1 (1982).
 [11] I. G. Kevrekidis, L. D. Schmidt, and R. Aris, *Chem. Eng. Sci.* **41**, 1263 (1986).
 [12] I. G. Kevrekidis, R. Aris, and L. D. Schmidt, *Chem. Eng. Sci.* **41**, 1549 (1986).
 [13] I. Schreiber, M. Dolnik, P. Choc, and M. Marek, *Phys. Lett. A* **128**, 66 (1988).
 [14] W. Vance and J. Ross, *J. Chem. Phys.* **91**, 7654 (1989).
 [15] B. B. Peckham, *Nonlinearity* **3**, 261 (1990).
 [16] B. B. Peckham and I. G. Kevrekidis, *SIAM J. Math. Anal.* **22**, 1552 (1991).
 [17] V. I. Arnold, *Chaos* **1**, 20 (1991).
 [18] E. Mosekilde, J. S. Thomsen, C. Knudsen, and R. Feldberg, *Physica D* **66**, 143 (1993).
 [19] T. Nomura, S. Sato, S. Doi, J. P. Segundo, and M. D. Stiber, *Biol. Cybern.* **72**, 55 (1994).
 [20] K. Yoshikawa, K. Fukunaga, and H. Kawakami, *Chem. Phys. Lett.* **174**, 203 (1990).
 [21] K. Yoshikawa, N. Oyama, M. Shoji, and S. Nakata, *Am. J. Phys.* **59**, 137 (1991).
 [22] S. Nakata, T. Miyata, N. Ojima, and K. Yoshikawa, *Physica D* **115**, 313 (1998).
 [23] K. Miyakawa and K. Yamada, *Physica D* **127**, 177 (1999).
 [24] K. Miyakawa and K. Yamada, *Physica D* **151**, 217 (2001).

- [25] M. R. Guevara, L. Glass, and A. Shrier, *Science* **214**, 1350 (1981).
- [26] M. Okamura and K. Yoshikawa, *Phys. Rev. E* **61**, 2445 (2000).
- [27] S. Martin, *Geophys. Fluid Dyn.* **1**, 143 (1970).
- [28] J. Walker, *Sci. Am.* **237**(4), 142 (1977).
- [29] P.-H. Alfredsson and T. Lagerstedt, *Phys. Fluids* **24**, 10 (1981).
- [30] R. M. Noyes, *J. Chem. Educ.* **66**, 207 (1989).
- [31] K. Yoshikawa, S. Nakata, M. Yamanaka, and T. Waki, *J. Chem. Educ.* **66**, 205 (1989).
- [32] S. Upadhyay, A. K. Das, V. Agarwala, and R. C. Srivastava, *Langmuir* **8**, 2567 (1992).
- [33] A. K. Das and R. C. Srivastava, *J. Chem. Soc., Faraday Trans.* **89**, 905 (1993).
- [34] O. Steinbock, A. Lange, and I. Rehberg, *Phys. Rev. Lett.* **81**, 798 (1998).
- [35] K. Aoki, *Physica D* **147**, 187 (2000).
- [36] R. P. Rastogi, R. C. Srivastava, and S. Kumar, *J. Colloid Interface Sci.* **283**, 139 (2005).
- [37] J. Dempster, *Computer Analysis of Electrophysiological Signals* (Academic Press, San Diego, 1993).
- [38] D. H. Perkel, J. H. Schulman, T. H. Bullock, G. P. Moore, and J. P. Segundo, *Science* **145**, 61 (1964).
- [39] M. R. Guevara and H. J. Jongsma, *Am. J. Physiol.* **258**, H734 (1990).
- [40] L. Glass and J. Sun, *Phys. Rev. E* **50**, 5077 (1994).
- [41] D. Singer, *SIAM J. Math. Anal.* **35**, 260 (1978).
- [42] H. G. Othmer and M. Xie, *J. Math. Biol.* **39**, 139 (1999).
- [43] E. N. Cytrynbaum, *J. Theor. Biol.* **229**, 69 (2004).
- [44] H. Croisier and P. C. Dauby, *J. Theor. Biol.* **246**, 430 (2007).
- [45] G. Steinbeck, R. Haberl, and B. Lüderitz, *Circ. Res.* **46**, 859 (1980).
- [46] M. R. Guevara and A. Shrier, *Ann. N.Y. Acad. Sci.* **591**, 11 (1990).
- [47] J. B. Nolasco and R. W. Dahlen, *J. Appl. Physiol.* **25**, 191 (1968).
- [48] M. R. Guevara, G. Ward, A. Shrier, and L. Glass, in *Computers in Cardiology 1984* (IEEE Computer Society Press, Silver Spring, MD, 1984), p. 167.
- [49] M. R. Guevara, F. Alonso, D. Jeandupeux, and A. C. G. van Ginneken, in *Cell to Cell Signalling: From Experiments to Theoretical Models*, edited by A. Goldbeter (Harcourt Brace Jovanovich, London, 1989), p. 551.
- [50] G. V. Savino, L. Romanelli, D. L. González, O. Piro, and M. E. Valentinuzzi, *Biophys. J.* **56**, 273 (1989).
- [51] D. R. Chialvo, R. F. Gilmour, Jr., and J. Jalife, *Nature (London)* **343**, 653 (1990).
- [52] A. Vinet, D. R. Chialvo, D. C. Michaels, and J. Jalife, *Circ. Res.* **67**, 1510 (1990).
- [53] N. F. Otani and R. F. Gilmour, Jr., *J. Theor. Biol.* **187**, 409 (1997).
- [54] G. M. Hall, S. Bahar, and D. J. Gauthier, *Phys. Rev. Lett.* **82**, 2995 (1999).
- [55] F. Hua and R. F. Gilmour, Jr., *Circ. Res.* **94**, 810 (2004).
- [56] T. J. Lewis and M. R. Guevara, *J. Theor. Biol.* **146**, 407 (1990).
- [57] A. Vinet and F. A. Roberge, *J. Theor. Biol.* **170**, 201 (1994).
- [58] J. J. Fox, E. Bodenschatz, and R. F. Gilmour, Jr., *Phys. Rev. Lett.* **89**, 138101 (2002).
- [59] C. Zemlin, E. Storch, and H. Herzog, *BioSystems* **66**, 1 (2002).
- [60] C. C. Mitchell and D. G. Schaeffer, *Bull. Math. Biol.* **65**, 767 (2003).
- [61] E. M. Cherry and F. H. Fenton, *Am. J. Physiol.* **292**, H43 (2007).
- [62] G. R. Mines, *J. Physiol. (London)* **46**, 349 (1913).
- [63] P. Bryant and C. Jeffries, *Physica D* **25**, 196 (1987).
- [64] M. Rivera, P. Parmananda, and M. Eiswirth, *Phys. Rev. E* **65**, 025201(R) (2002).
- [65] C. Knudsen, J. Sturis, and J. S. Thomsen, *Phys. Rev. A* **44**, 3503 (1991).
- [66] G. Mayer-Kress and H. Haken, *Physica D* **10**, 329 (1984).
- [67] H. Arce, A. López, and M. R. Guevara, *Chaos* **12**, 807 (2002).
- [68] R. Perez and L. Glass, *Phys. Lett.* **90**, 441 (1982).
- [69] L. Glass and J. Bélair, in *Nonlinear Oscillations in Biology and Chemistry*, edited by H. G. Othmer (Springer, New York, 1986), p. 232.
- [70] J. Finkeová, M. Dolnik, B. Hrudka, and M. Marek, *J. Phys. Chem.* **94**, 4110 (1990).
- [71] J. Farjas, R. Herrero, F. Pi, and G. Orriols, *Int. J. Bifurcation Chaos Appl. Sci. Eng.* **8**, 1413 (1998).
- [72] A. R. Yehia, D. Jeandupeux, F. Alonso, and M. R. Guevara, *Chaos* **9**, 916 (1999).
- [73] H. González, A. Torres, C. Lerma, G. Arriola, G. Pastelin, and H. Arce, *Arch. Inst. Cardiol. Mex.* **74**, 11 (2004).
- [74] C. Hayashi, *Nonlinear Oscillations in Physical Systems* (McGraw-Hill, New York, 1964).
- [75] D. L. Gonzalez and O. Piro, *Phys. Rev. Lett.* **50**, 870 (1983).
- [76] D. G. Aronson, R. P. McGehee, I. G. Kevrekidis, and R. Aris, *Phys. Rev. A* **33**, 2190 (1986).
- [77] E. J. Ding, *Phys. Rev. A* **36**, 1488 (1987).
- [78] V. C. Kowtha, A. Kunysz, J. R. Clay, L. Glass, and A. Shrier, *Prog. Biophys. Mol. Biol.* **61**, 255 (1994).
- [79] N. Inaba, R. Fujimoto, H. Kawakami, and T. Yoshinaga, *Electron. Commun. Jpn., Part 2: Electron.* **83**, 35 (2000).
- [80] M. Sekikawa, N. Inaba, T. Yoshinaga, and H. Kawakami, *Electron. Commun. Jpn., Part 2: Electron.* **87**, 30 (2004).
- [81] A. T. Winfree, *J. Math. Biol.* **1**, 73 (1974).
- [82] M. R. Guevara, L. Glass, M. C. Mackey, and A. Shrier, *IEEE Trans. Syst. Man Cybern.* **13**, 790 (1983).
- [83] A. Campbell, A. Gonzalez, D. L. Gonzalez, O. Piro, and H. A. Larrondo, *Physica A* **155**, 565 (1989).
- [84] T. Krogh-Madsen, L. Glass, E. J. Doedel, and M. R. Guevara, *J. Theor. Biol.* **230**, 499 (2004).
- [85] D. G. Tsalikakis, H. G. Zhang, D. I. Fotiadis, G. P. Kremmydas, and L. K. Michalis, *Comput. Biol. Med.* **37**, 8 (2007).
- [86] J. Bélair and L. Glass, *Physica D* **16**, 143 (1985).
- [87] M. Feingold, D. L. Gonzalez, O. Piro, and H. Viturro, *Phys. Rev. A* **37**, 4060 (1988).
- [88] J. C. Alexander, E. J. Doedel, and H. G. Othmer, *SIAM J. Math. Anal.* **50**, 1373 (1990).
- [89] S.-G. Lee and S. Kim, *Phys. Rev. E* **73**, 041924 (2006).
- [90] P. S. Linsay, *Phys. Rev. Lett.* **47**, 1349 (1981).
- [91] G. H. Gunaratne, P. S. Linsay, and M. J. Vinson, *Phys. Rev. Lett.* **63**, 1 (1989).
- [92] H. Arce, A. Xu, H. González, and M. R. Guevara, *Chaos* **10**, 411 (2000).
- [93] J. C. Robinson, *Chaos* **5**, 330 (1995).
- [94] Y. Shiferaw, M. A. Watanabe, A. Garfinkel, J. N. Weiss, and A. Karma, *Biophys. J.* **85**, 3666 (2003).
- [95] www.instrutech.com
- [96] www.bruyton.com